First-principles study of binary bcc alloys using special quasirandom structures

Chao Jiang,[1] C. Wolverton,[2] Jorge Sofo,[1,3,4] Long-Qing Chen,[1] and Zi-Kui Liu[1]
[1]*Department of Materials Science and Engineering, The Pennsylvania State University, University Park, Pennsylvania 16802, USA*
[2]*Ford Research and Advanced Engineering, MD3083/SRL, Dearborn, Michigan 48121-2053, USA*
[3]*Materials Research Institute, The Pennsylvania State University, University Park, Pennsylvania 16802, USA*
[4]*Department of Physics, The Pennsylvania State University, University Park, Pennsylvania 16802, USA*
(Received 29 October 2003; revised manuscript received 27 January 2004; published 28 June 2004)

We present three 16-atom special quasirandom structures (SQS's) for $A_{1-x}B_x$ bcc substitutional alloys at compositions $x=0.25$, 0.50 and 0.75, respectively. The structures possess local pair and multisite correlation functions that mimic those of the corresponding random bcc alloy. The introduction of these SQS's allows for the possibility of first-principles calculations of bcc solid solutions, even those with significant size-mismatch or atomic relaxation. We have tested our SQS's via first-principles calculations in the Mo–Nb, Ta–W and Cr–Fe systems, in which the bcc solid solution is observed to be stable over the whole composition range. Our first-principles SQS results provide formation enthalpies, equilibrium lattice parameters and magnetic moments of these bcc alloys which agree satisfactorily with most existing experimental data in the literature. In an effort to understand the atomic relaxation behavior in bcc solid solutions, we have also investigated the nearest neighbor bond length distributions in the random bcc alloys. The proposed bcc SQS's are quite general and can be applied to other binary bcc alloys.

DOI: 10.1103/PhysRevB.69.214202 PACS number(s): 61.66.Dk

I. INTRODUCTION

First-principles calculations based on density functional theory[1] are now routinely used to predict the thermodynamic, structural, magnetic, electrical, and optical properties of a wide range of materials. These methods are truly predictive since only atomic numbers and crystal structure information are needed as input. As many of these methods rely on the construction of cells with periodic boundary conditions, the calculations are fairly straightforward for perfectly-ordered stoichiometric compounds. However, the situation is more complicated when treating disordered solid solutions.

One way to treat random $A_{1-x}B_x$ solid solutions would be to construct a large supercell and randomly decorate the host lattice with A and B atoms. Such an approach would necessarily require very large supercells to adequately mimic the statistics of the random alloy. Since density functional methods are computationally constrained by the number of atoms that one can treat, this brute-force approach could be computationally prohibitive. Hence, researchers have searched for more elegant theories to treat a disorder, often in an average or mean-field sense: The coherent potential approximation[2] (CPA) is such a mean-field approach which treats random $A_{1-x}B_x$ alloys by considering the average occupations of lattice sites by A and B atoms. The dependence of properties on the *local* environments surrounding atoms is therefore not treated explicitly in CPA. However, in a real (non-mean-field) random alloy, there exists a distribution of local environments (e.g., A or B surrounded by the various A_mB_{8-m} coordination shells with m between 0 and 8 in bcc alloys), resulting in local environmentally-dependent quantities such as charge transfer and local displacements of atoms from their ideal lattice positions.[3–7] Experimental observations[8] also show that, even in random $A_{1-x}B_x$ solid solutions, the average A–A, A–B and B–B bond lengths are generally different. In size-mismatched semiconductor alloys, such local atomic relaxations have been shown to significantly affect their thermodynamic and electronic properties.[3–6]

The concept of special quasirandom structures (SQS's) was proposed by Zunger *et al.*[3,4,9] to overcome the limitations of mean-field theories, but without the prohibitive computational cost associated with directly constructing large supercells with the random occupancy of atoms. SQS's are specially designed *small-unit-cell* periodic structures with only a few (2–16) atoms per unit cell, which closely mimic the most relevant, near-neighbor pair and multisite correlation functions of the random substitutional alloys. Since the SQS approach is not a mean-field one, a distribution of distinct local environments is maintained, the average of which corresponds to the random alloy. Thus, a single DFT calculation of an SQS can give many important alloy properties[3,4,9] (e.g., equilibrium bond lengths, charge transfer, formation enthalpies, etc.) which depend on the existence of those distinct local environments. Furthermore, since the SQS approach is geared towards relatively small-unit-cells, essentially any DFT method can be applied to this approach, including full-potential methods capable of accurately capturing the effects of atomic relaxation.

The SQS approach has been used extensively to study the formation enthalpies, bond length distributions, density of states, band gaps and optical properties in semiconductor alloys.[3,4,9] They have also been applied to investigate the local lattice relaxations in size-mismatched transition metal alloys[5–7,10] and to predict the formation enthalpies of Al-based fcc alloys.[11] However, to date, all the applications of the SQS methodology are for systems in which the substitutional alloy problem is fcc-based (e.g., fcc-based metals, zinc-blende-based semiconductors, or rock-salt-based oxides). No SQS's for the bcc structure exist in the literature. Therefore, in this work, we develop three SQS's for binary bcc alloys at compositions $x=0.25$, 0.50 and 0.75, respec-

tively. We demonstrate the usefulness of the present SQS's by applying them to the Mo–Nb, Ta–W and Cr–Fe systems, in which the bcc structure is known to be stable over the whole composition range. We also compare the predicted formation enthalpies, equilibrium lattice parameters and magnetic moments of the bcc alloys with the existing experimental data in the literature.

II. GENERATION OF SPECIAL QUASIRANDOM STRUCTURES

For a binary $A_{1-x}B_x$ substitutional alloy, many properties are dependent on the *configuration*, or the substitutional arrangement of A and B atoms on the lattice type. These configurationally-dependent properties (such as the energy) can be characterized very efficiently by a "lattice algebra":[3–6] Pseudo-spin variables are assigned to each site, $S_i=-1(+1)$ if an A (B) atom sits at site i. We further define geometric figures, f, symmetry-related groupings of lattice sites, e.g., single site, nearest-neighbor pair, three-body figures, etc. These figures, $f=(k,m)$ can have k vertices and span a maximum distance of m ($m=1,2,3\ldots$, are the first, second and third-nearest neighbors, etc.). By taking the product of the spin variables over all sites of a figure, and averaging over all symmetry-equivalent figures of the lattice, we obtain the correlation functions $\overline{\Pi}_{k,m}$.[3,4] For the perfectly random $A_{1-x}B_x$ bcc alloys, there is no correlation in the occupation between various sites, and therefore $\overline{\Pi}_{k,m}$ simply becomes the product of the lattice-averaged site variable, which is related to the composition by $\langle S_i\rangle=2x-1$. Thus, for the perfectly random alloy, the pair and multisite correlation functions $\overline{\Pi}_{k,m}$ are given quite simply as $\langle\overline{\Pi}_{k,m}\rangle_R=(2x-1)^k$.

The SQS approach amounts to finding small-unit-cell ordered structures that possess $(\overline{\Pi}_{k,m})_{\mathrm{SQS}}\cong\langle\overline{\Pi}_{k,m}\rangle_R$ for as many figures as possible. Admittedly, describing random alloys by small unit-cell periodically-repeated structures will surely introduce erroneous correlations beyond a certain distance. However, since interactions between nearest neighbors are generally more important than interactions between more distant neighbors, we can construct SQS's that exactly reproduce the correlation functions of a random alloy between the first few nearest neighbors, deferring errors due to periodicity to more distant neighbors.

In the present study, we have generated various SQS-N structures (with $N=2$, 4, 8 and 16 atoms per unit cell) for the random bcc alloys at composition $x=0.50$ and 0.75 using the *gensqs* code in the Alloy-Theoretic Automated Toolkit (ATAT).[12] For each composition x, our procedure can be described as follows: (1) Using *gensqs*, we exhaustively generate all structures based on the bcc lattice with N atoms per unit cell and composition x. (2) We then construct the pair and multisite correlation functions $\overline{\Pi}_{k,m}$, for each structure. (3) Finally, we search for the structure (s) that best match the correlation functions of random alloys over a specified set of pair and multisite figures. We obtained the SQS-16 structure for $x=0.5$ by requiring that its pair correlation functions be identical to those of the random alloy up to the fifth-nearest neighbor. However, for $x=0.75$, no SQS-16 structures satisfy this criterion. Therefore, we instead chose a structure whose pair correlation functions are identical to the random alloy up to the fourth-nearest neighbor. The other SQS-N structures with $N=2$, 4 and 8 atoms per unit cell were generated using an analogous approach. Of course, in general, the smaller the unit cell SQS-N, the fewer pair correlations that match those of the random alloy.

The lattice vectors and atomic positions of the obtained SQS-N structures in their ideal, unrelaxed forms are given in Table I, all in Cartesian coordinates. The definitions of the multisite figures considered here are given in Table II. In Table III, the pair and multisite correlation functions of the SQS-N structures presented in Table I are compared with those of the corresponding random alloys. We also give an estimate of the errors due to periodicity, estimated as $\Sigma_{m=1}^{4}(\overline{\Pi}_{2,m}-(2x-1)^2)^2$, over the first four neighbor pairs. These errors are also shown in Table III, and they rapidly decrease with increasing N. We note that the SQS-N structures for $x=0.25$ are obtained simply by switching the A and B atoms in SQS-N for $x=0.75$. Since this amounts to replacing all of the spin variables by $S_i\rightarrow -S_i$, all even-body correlations are equivalent for $x=0.25$ and $x=0.75$, while all odd-body correlations simply change sign. Thus, the three-body figures are largely responsible for asymmetries in the formation energies between $x=0.25$ and $x=0.75$.

In all present calculations, unless specifically noted, we use the 16-atom SQS's to represent the random bcc alloys. The extent to which they match the random alloy correlations is comparable to those of the existing 16-atom SQS's for the fcc structure, which reproduce the pair correlation functions of perfectly random fcc alloys accurately up to the seventh-nearest neighbor at $x=0.5$ and third-nearest neighbor at $x=0.75$.[11] SQS-16 for $x=0.5$ is a triclinic-type structure with space group $P\bar{1}$ (space group No. 2 in the International Tables of Crystallography), and SQS-16 for $x=0.75$ is a monoclinic-type structure with space group Cm (space group No. 8 in the International Tables of Crystallography).[13] Their pictures are also given in Fig. 1 in their ideal, unrelaxed forms.

III. FIRST-PRINCIPLES METHODOLOGY

First-principles calculations were performed using the plane wave method with Vanderbilt ultrasoft pseudopotentials,[14,15] as implemented in the highly-efficient Vienna *ab initio* simulation package (VASP).[16,17] We used the generalized gradient approximation (GGA)[18] since we have included Cr–Fe in our list of systems to test the SQS's: The local density approximation (LDA) is known to incorrectly predict the ground state of Fe to be a nonmagnetic close-packed phase, whereas GGA calculations correctly predict the ground state to be the ferromagnetic bcc phase.[19] The k-point meshes for Brillouin zone sampling were constructed using the Monkhorst-Pack scheme[20] and the total number of k-points times the total number of atoms per unit cell was at least 6000 for all systems. A plane wave cutoff energy E_{cut} of 233.1, 235.2 and 296.9 eV were used for the Mo–Nb, Ta–W and Cr–Fe system, respectively. All calculations include sca-

TABLE I. Structural descriptions of the SQS-*N* structures. Lattice vectors and atomic positions are given in Cartesian coordinates, in units of *a*, the bcc lattice parameter. Atomic positions are given for the ideal, unrelaxed bcc sites.

	$x=0.5$	$x=0.75$
SQS-16	Lattice vectors	Lattice vectors
	$\vec{a}_1=(-0.5,-1.5,-2.5),\vec{a}_2=(-0.5,2.5,1.5)$	$\vec{a}_1=(1.0,-2.0,0.0),\vec{a}_2=(0.0,-2.0,1.0)$
	$\vec{a}_3=(1.5,0.5,-0.5)$	$\vec{a}_3=(-2.0,0.0,-2.0)$
	Atomic positions	Atomic positions
	A−(0.0,0.0,−2.0),A−(0.5,1.5,−0.5)	A−(0.0,−4.0,0.0),A−(0.0,−2.0,0.0)
	A−(1.0,0.0,−2.0),A−(0.5,0.5,−0.5)	A−(0.5,−2.5,0.5),A−(0.5,−3.5,0.5)
	A−(0.5,−0.5,−2.5),A−(−0.5,1.5,−0.5)	B−(−1.5,−0.5,−1.5),B−(−1.5,−1.5,−1.5)
	A−(0.0,2.0,0.0),A−(0.5,2.5,0.5)	B−(−1.0,−1.0,−1.0),B−(−0.5,−0.5,−0.5)
	B−(1.0,2.0,0.0),B−(−0.5,0.5,−1.5)	B−(−1.0,−4.0,−1.0),B−(−1.0,−2.0,−1.0)
	B−(1.0,1.0,−1.0),*B*−(0.0,1.0,0.0)	B−(−0.5,−1.5,−0.5),B−(0.0,−1.0,0.0)
	B−(0.5,1.5,−1.5),B−(0.0,1.0,−1.0)	B−(−1.0,−3.0,−1.0),B−(−0.5,−2.5,−0.5)
	B−(0.0,0.0,−1.0),B−(0.5,0.5,−1.5)	B−(−0.5,−3.5,−0.5),B−(0.0,−3.0,0.0)
SQS-8	$\vec{a}_1=(0.5,0.5,-1.5),\vec{a}_2=(1.5,0.5,-0.5)$	$\vec{a}_1=(-1.0,0.0,0.0),\vec{a}_2=(0.0,1.0,-1.0),$
	$\vec{a}_3=(0.0,-2.0,0.0)$	$\vec{a}_3=(0.0,-2.0,-2.0)$
	A−(2.0,0.0,−2.0),A−(0.5,−1.5,−0.5)	A−(−0.5,−0.5,−1.5),A−(−1.0,−1.0,−2.0)
	A−(1.0,−1.0,−1.0),A−(1.5,−0.5,−1.5)	B−(−0.5,−1.5,−2.5),B−(−0.5,0.5,−1.5)
	B−(2.0,−1.0,−2.0),B−(0.5,−0.5,−0.5)	B−(−1.0,−1.0,−3.0),B−(−1.0,0.0,−1.0)
	B−(1.0,0.0,−1.0),B−(1.5,0.5,−1.5)	B−(−0.5,−0.5,−2.5),B−(−1.0,0.0,−2.0)
SQS-4	$\vec{a}_1=(-0.5,0.5,0.5),\vec{a}_2(0.0,-1.0,1.0)$	$\vec{a}_1=(-0.5,0.5,0.5),\vec{a}_2=(0.0,-1.0,1.0)$
	$\vec{a}_3=(1.5,0.5,0.5)$	$\vec{a}_3=(1.5,0.5,0.5)$
	A−(0.5,−0.5,1.5),A−(1.0,0.0,1.0)	A−(1.0,0.0,1.0),B−(0.0,0.0,1.0)
	B−(0.0,0.0,1.0),B−(1.0,0.0,2.0)	B−(1.0,0.0,2.0),B−(0.5,−0.5,1.5)
SQS-2	$\vec{a}_1=(-0.5,0.5,-0.5),\vec{a}_2=(-0.5,-0.5,0.5)$	
	$\vec{a}_3=(0.0,1.0,1.0)$	
	A−(−1.0,1.0,1.0),B−(−0.5,0.5,0.5)	

lar relativistic corrections (i.e., no spin–orbit interaction).

Spin-polarized calculations were performed for the Cr–Fe alloys, whereas all other calculations were nonmagnetic. Pure bcc Fe is ferromagnetic while pure bcc Cr is antiferromagnetic with incommensurate spin density waves[21]. This leads to quite a complicated magnetic structure in the $Cr_{1-x}Fe_x$ bcc alloys at low temperatures,[22] which was not investigated in the present study. Instead, since our SQS calculations were performed at compositions $x=0.25$, 0.5 and 0.75, all larger than the critical composition $x=0.2$ beyond which the $Cr_{1-x}Fe_x$ bcc alloy becomes ferromagnetic,[23] we assumed a ferromagnetic structure for the Cr–Fe bcc alloys in our spin-polarized calculations.

By computing the quantum-mechanical forces and stress tensor, structural and atomic relaxations were performed and all atoms were relaxed into their equilibrium positions using a conjugate-gradient scheme. For the bcc alloys considered in the present study, the SQS's were fully relaxed with respect to both the volume and shape of the unit cell as well as all the atomic positions. In all our calculations, the magnitudes of cell vector distortions of the fully relaxed SQS's with respect to their ideal, unrelaxed unit cells are very small, indicating structural stability of the bcc lattice for these systems.

We obtained the formation enthalpies of the random bcc alloys as

$$\Delta H(x) = E(A_{1-x}B_x) - (1-x)E(A) - xE(B), \qquad (1)$$

where $E(A)$, $E(B)$, and $E(A_{1-x}B_x)$ are the first-principles calculated total energies of the constituent pure elements A and B and the corresponding SQS, respectively, each relaxed to

TABLE II. Vertices of the multisite figures, given in units of *a*, the bcc lattice parameter.

Type	Figure designation	Vertices			
Triplets	(3,2)	(0, 0, 0)	(0.5, 0.5, 0.5)	(0.5,−0.5,0.5)	
	(3,3)	(0, 0, 0)	(0.5, 0.5, 0.5)	(1, 0, 1)	
Quadruplets	(4,2)	(0, 0, 0)	(0.5, 0.5, 0.5)	(0.5,−0.5,0.5)	(1, 0, 0)

TABLE III. Pair and multisite correlation functions of SQS-*N* structures. The number in the square brackets next to $\overline{\Pi}_{k,m}$ gives the degeneracy factor of the corresponding figure.

			x=0.5				x=0.75		
	Random	SQS-16	SQS-8	SQS-4	SQS-2	Random	SQS-16	SQS-8	SQS-4
$\overline{\Pi}_{2,1}[4]$	0	0	0	0	0	0.25	0.25	0.25	0.25
$\overline{\Pi}_{2,2}[3]$	0	0	0	−0.3333	−0.3333	0.25	0.25	0.3333	0
$\overline{\Pi}_{2,3}[6]$	0	0	−0.1667	0	−0.3333	0.25	0.25	0.1667	0.1667
$\overline{\Pi}_{2,4}[12]$	0	0	0	0	0	0.25	0.25	0.25	0.25
$\overline{\Pi}_{2,5}[4]$	0	0	−0.5	0	1	0.25	0.125	0.5	0.5
$\overline{\Pi}_{2,6}[3]$	0	−0.3333	0.3333	−0.3333	1	0.25	0.0833	0.3333	0.3333
$\overline{\Pi}_{2,7}[12]$	0	0	0	0	0	0.25	0.25	0.25	0.25
$\overline{\Pi}_{3,2}[12]$	0	0	0	0	0	0.125	0.1667	0.1667	0
$\overline{\Pi}_{3,3}[12]$	0	0	0	0	0	0.125	0.0833	0.1667	0.1667
$\overline{\Pi}_{4,2}[6]$	0	0	−0.3333	−0.3333	−0.3333	0.0625	0.1667	0	0
Error	0	0	0.0278	0.1111	0.2222	0	0	0.0139	0.0694

their equilibrium geometries. In the present study, all elements considered are observed at low temperature in the bcc structure, and thus, pure element bcc energies were used as reference states in Eq. (1).

To study the local atomic relaxations, the distributions of nearest neighbor bond lengths in the random bcc alloys were also obtained from the relaxed SQS's. Since in a perfect bcc structure each atom is coordinated by eight nearest neighbors, we have taken the smallest eight interatomic distances of each atom in the relaxed SQS's to be representative of the nearest neighbor bonds.We then categorized the bond distances into different bond types, e.g., A–A, A–B and B–B, and computed the average bond lengths for each type.

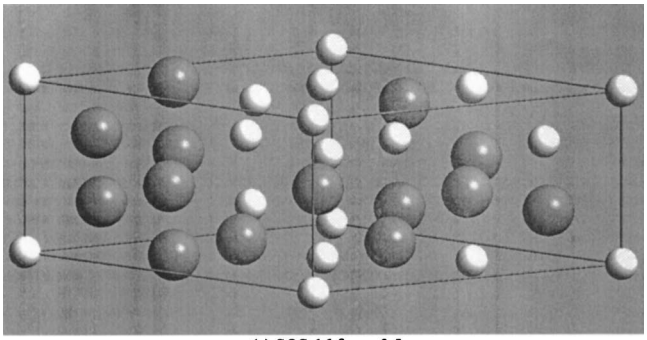

(a) SQS-16 for x=0.5

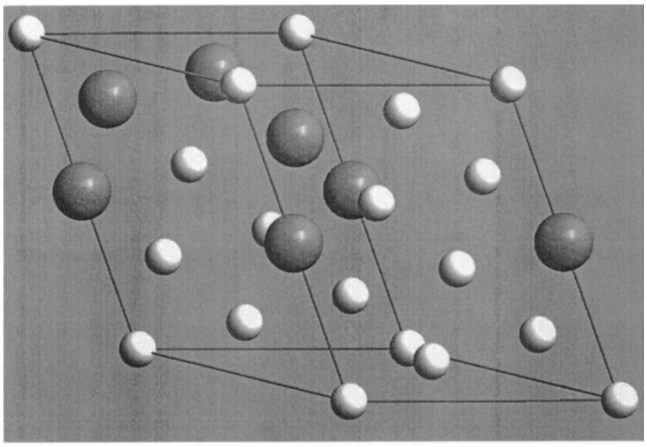

(b) SQS-16 for x=0.75

FIG. 1. Crystal structure of the SQS-16 structures in their ideal, unrelaxed forms. Dark and light spheres represent A and B atoms, respectively.

IV. RESULTS AND DISCUSSIONS

A. Pure elements

The first-principles calculated $T=0$ K lattice parameters of bcc Nb, Mo, Ta, W, Cr and Fe, each relaxed to their equilibrium volumes, are given in Table IV. Both spin-polarized and non-spin-polarized calculations were performed for bcc Cr and Fe. Consistent with previous DFT studies, ferromagnetism substantially stabilizes the bcc Fe (energy is decreased by ~0.56 eV/atom upon the inclusion of spin polarization), making it the ground state of Fe. Spin-polarized, ferromagnetic calculations for Cr resulted in a nonmagnetic solution. According to Table IV, the lattice mismatch (defined as $\Delta a/\overline{a}$) in the Mo–Nb, Ta–W, and Cr–Fe alloy systems are found to be 4.3%, 3.7% and 0%, respectively.

B. Mo–Nb

Mo and Nb form a continuous bcc solid solution. No intermediate phases have been reported in this system.[24] The

TABLE IV. First principles (VASP–GGA) calculated equilibrium lattice parameter for pure elements in the bcc structure. Spin-polarized calculations were performed for Cr and Fe in their ferromagnetic (FM) state.

Element	Mo	Nb	Ta	W	Cr (FM)	Fe (FM)
a (Å)	3.15	3.29	3.29	3.17	2.85	2.85

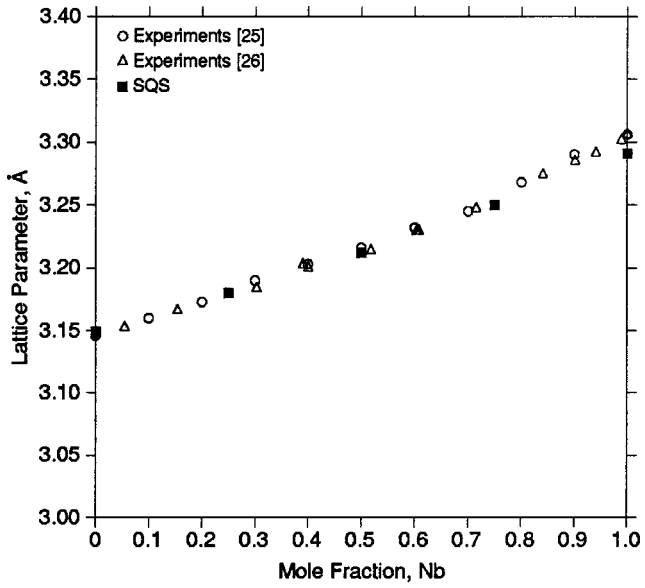

FIG. 2. Equilibrium lattice parameters of Mo–Nb bcc alloys as a function of composition.

equilibrium lattice parameters of Mo–Nb bcc alloys obtained from the relaxed SQS's are plotted in Fig. 2 together with those of the pure bcc Mo and Nb given in Table IV. The experimental measurements by Goldschmidt and Brand[25] and Catterall and Barker[26] are also included for comparison. Our calculations are in good agreement with experiments. Both show a small negative deviation from the Vegard's law, i.e., $a(A_{1-x}B_x)=(1-x)a(A)+xa(B)$, where $a(A_{1-x}B_x)$, $a(A)$ and $a(B)$ are the equilibrium lattice parameters of alloy $A_{1-x}B_x$ and constituent pure elements A and B, respectively. In Fig. 3, the predicted formation enthalpies of random Mo–Nb bcc alloys are compared with the experimental measurements by Singhal and Worrell[24] at 1200 K using a solid state galvanic cell. Fairly satisfactorily agreement has been reached with the largest discrepancy less than 2 kJ/mol. Sigli *et al.*[27] also calculated the formation enthalpies of Mo–Nb bcc alloys using the TB–CPA–GPM approach. For the purpose of comparison, their results are also shown in Fig. 3, which agree quite well with our SQS's results. In all three cases, the asymmetry of the formation enthalpy with respect to $x=0.50$ is quite small.

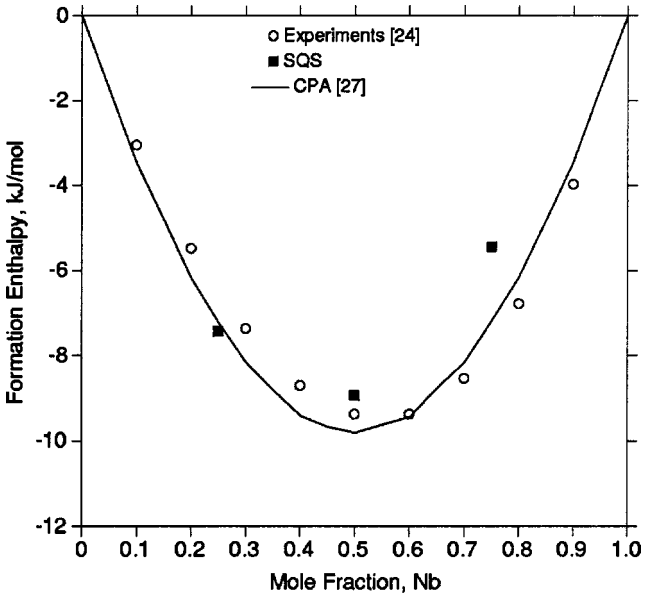

FIG. 3. Formation enthalpies of Mo–Nb bcc alloys as a function of composition.

The negative formation enthalpies indicate that Mo–Nb is an ordering-type system. Sigli *et al.*[27] predicted that an ordered B2 structure is stable in Mo–Nb below 830 K. Neglecting the effects of vibrational entropy and assuming an ideal configurational entropy of mixing for the $Mo_{1-x}Nb_x$ bcc solid solution, i.e., $\Delta S_{\text{ideal}}=-R(x\ln(x)+(1-x)\ln(1-x))$, we obtain a crude estimate the A2–B2 order–disorder transition temperature at composition $x=0.5$ in Mo–Nb using the following equation:

$$T_c \approx \frac{\Delta H_{\text{bcc}}^{\text{SQS}}(x=0.5)-\Delta H_{\text{B2}}}{R\ln 2}. \tag{2}$$

Our first-principles calculation of the formation enthalpy of the fully ordered MoNb B2 structure gives −13.1 kJ/mol. Using Eq. (2), we thus obtain $T_c \approx 731$ K, in good agreement with the temperature of 830 K predicted by Sigli *et al.* [27] Since this temperature is relatively low compared with the melting temperature of Mo (2896 K) and Nb (2750 K), sluggish kinetics might explain why the B2 structure or other ordered phases have not been observed experimentally. However, our results do predict the existence of ordered structures in Mo–Nb which to date have not yet been observed. Therefore, we assert that experimental re-examination of the low-temperature phase stability of Mo–Nb would be of interest.

C. Ta–W

Ta and W also form a continuous bcc solid solution with no intermediate phases.[28] The predicted equilibrium lattice parameters of Ta–W bcc alloys are shown in Fig. 4, in good agreement with the existing experimental measurements.[29] Both show a negative deviation from Vegard's law. In Fig. 5, the predicted formation enthalpies of random Ta–W bcc alloys are compared with the experimental solid state galvanic cell measurements of Singhal and Worrell.[28] In Figs. 4 and 5 we also show the formation enthalpies of random Ta–W bcc alloys calculated by Turchi *et al.*[30] using the TB–LMTO–ASA–CPA approach. Interestingly, although experimental formation enthalpies exhibit a strong asymmetry towards the Ta-rich side, both SQS and CPA calculated formation enthalpies exhibit a strong asymmetry towards the W-rich side. Such large discrepancies between our calculations and experimental measurements on the W-rich side may be due to the slow kinetics at the experimental temperature of 1200 K, which makes thermodynamic equilibrium difficult to reach, as was also pointed out by Turchi *et al.*[30] To investigate this hypothesis, we examined the tracer diffusivity of Ta in bcc W at 1200 K using the Arrhenius relation $D_{\text{Ta}}^{\text{W}}=6.2\times10^{-4}\text{Exp}(-601241/\text{RT})$ obtained by Arkhipova *et al.*[31] and obtained an extremely low value of 4.186×10^{-30} m^2/s. The

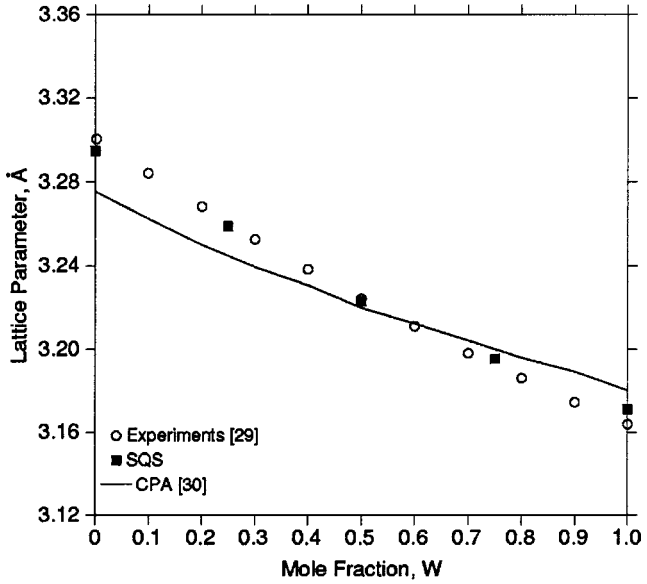

FIG. 4. Equilibrium lattice parameters of Ta–W bcc alloys as a function of composition.

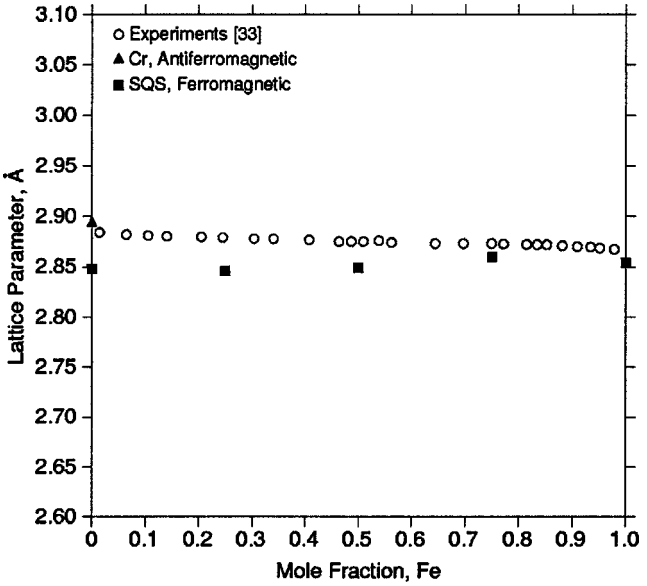

FIG. 6. Equilibrium lattice parameters of Cr–Fe bcc alloys as a function of composition.

fact that $D_{\mathrm{Ta}}^{\mathrm{W}}$ dominates the interdiffusion coefficients in the W-rich Ta–W bcc alloys could explain why the discrepancies between SQS calculations and experiments are largest on the W-rich side. However, we should also note other possibilities to explain this discrepancy: (1) Our SQS are constructed to mimic the perfectly random state, and thus short-range order in these alloys could also contribute to the discrepancy. (2) Although the SQS possess many pair and multibody correlations that match the random alloy statistics, there are deviations from the random alloy correlations for longer-ranged pair and other multibody interactions. If some of these interactions are significant, they could contribute to the discrepancy. (3) Finally, we should note that experimental measurements of formation enthalpies down to an accuracy of 1 kJ/mole are quite difficult, and it is possible that the experimental data is partly responsible for the discrepancy.

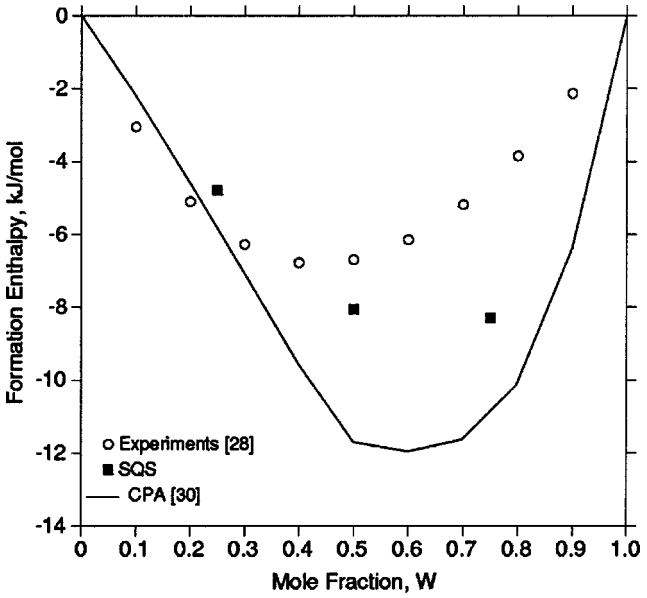

FIG. 5. Formation enthalpies of Ta–W bcc alloys as a function of composition.

It is interesting that the results of Turchi *et al.*[30] overestimate the formation enthalpies relative to our SQS results even though their CPA calculations ignore such important physical effects as atomic relaxations, which will lower the formation enthalpy. We attribute such apparent discrepancies to the atomic sphere approximation (ASA) employed in their CPA calculations.

The negative formation enthalpies indicate that Ta–W is also an ordering-type system. Turchi *et al.*[30] predicted that the Ta–W bcc alloys have a strong tendency toward B2 ordering. In the present study, we obtained via first-principles calculations the formation enthalpy of the fully ordered TaW B2 structure to be −11.2 kJ/mol. Assuming an ideal configurational entropy of mixing, the A2–B2 order-disorder transition temperature at composition $x=0.5$ in Ta–W is thus estimated using Eq. (2) to be $T_c \approx 552$ K, which is substantially lower than the temperatures predicted by Turchi *et al.*[30] The low order–disorder transition temperature could again explain why the B2 structure has not been observed experimentally in Ta–W. But again, our calculations predict the (low temperature) existence of ordered structures in the Ta–W system that have previously not been reported, and therefore future experimental work on this system would be of interest.

D. Cr–Fe

Cr and Fe form a continuous bcc solid solution with a miscibility gap appearing at low temperatures.[32] A sigma phase also forms at intermediate temperatures.[32] In Fig. 6, the predicted equilibrium lattice parameters of ferromagnetic Cr–Fe bcc alloys are compared with available experiments.[33] Figure 7 also gives the predicted magnetic moments (in μ_{B}

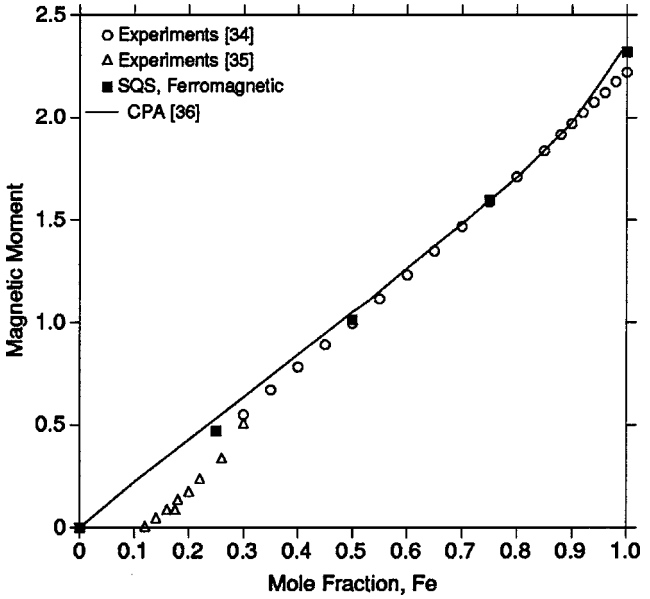

FIG. 7. Magnetic moment of Cr–Fe bcc alloys as a function of composition.

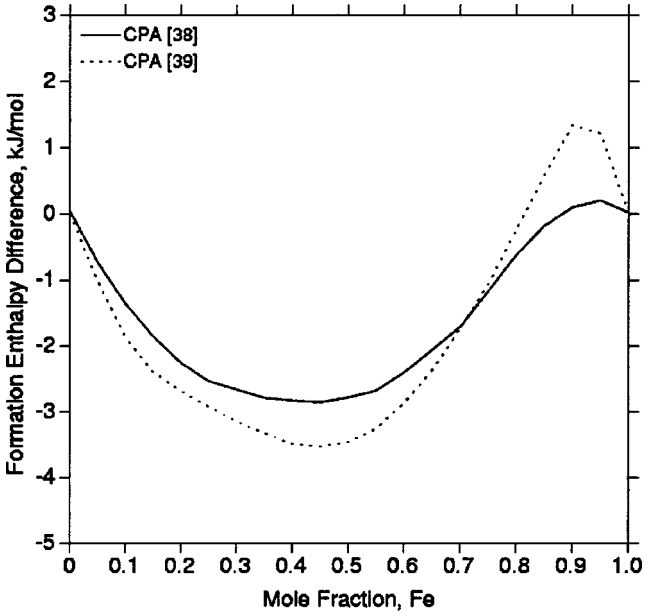

FIG. 8. CPA calculated formation enthalpy difference between the paramagnetic and ferromagnetic states of Cr–Fe bcc alloys.

per atom) of random ferromagnetic Cr–Fe bcc alloys together with the available experiments[34,35] and the calculated KKR–CPA results by Kulikov and Demangeat.[36] In both cases, the discrepancies near the Cr corner are due to the fact that we treat Cr as ferromagnetic instead of antiferromagnetic. In Fig. 6, we also include our calculated equilibrium lattice parameter of antiferromagnetic bcc Cr with a commensurate wave vector using a B2 unit cell, which is in good agreement with the measured value. We found that antiferromagnetism lowers the energy of bcc Cr by ~ 0.046 eV/atom.

Dench[37] experimentally measured the formation enthalpies of bcc Cr–Fe alloys at 1400 K. This temperature is well above the Curie (or Néel) temperature of Cr–Fe bcc alloys,[32] therefore, the measured alloys were all in the paramagnetic state. However, the present spin-polarized calculations correspond to the ferromagnetic state of the alloys. Akai and Dederichs[38] and Olsson *et al.*[39] calculated using the KKR–CPA and FCD–EMTO–CPA approach, respectively, the structural energy differences between the paramagnetic and ferromagnetic states of random Cr–Fe bcc alloys, $\Delta E^{\mathrm{FM}\rightarrow\mathrm{PM}}$, which are found to be substantial in the Cr–Fe system. In both studies, the disordered local moment (DLM) model was used, which treats the paramagnetic $\mathrm{Cr}_{1-x}\mathrm{Fe}_x$ alloy as a random quaternary $(\mathrm{Cr}\uparrow,\mathrm{Cr}\downarrow)_{1-x}(\mathrm{Fe}\uparrow,\mathrm{Fe}\downarrow)_x$ system with equal number of up-spin and down-spin atoms. Since the Cr–Fe system is a perfectly lattice-matched system with $\Delta a/\bar{a}<1\%$, one might expect that the atomic relaxations are small, and that the neglect of them in the CPA should represent only a minor approximation. We will investigate more the relaxation behavior of this alloy below.

Figure 8 shows the CPA calculated formation enthalpy difference between the paramagnetic and ferromagnetic states of Cr–Fe bcc alloys,[38,39] defined as

$$\Delta H^{\mathrm{FM}\rightarrow\mathrm{PM}}(x) = \Delta E^{\mathrm{FM}\rightarrow\mathrm{PM}}(\mathrm{A}_{1-x}\mathrm{B}_x) - (1-x)\Delta E^{\mathrm{FM}\rightarrow\mathrm{PM}}(\mathrm{A}) - x\Delta E^{\mathrm{FM}\rightarrow\mathrm{PM}}(\mathrm{B}). \quad (3)$$

By adding $\Delta H^{\mathrm{FM}\rightarrow\mathrm{PM}}$ to our SQS calculated formation enthalpies of ferromagnetic Cr–Fe bcc alloys, we obtain the formation enthalpy in the paramagnetic state. Our results are shown in Fig. 9 together with the corresponding experimental data[37] and the CPA DLM results by Olsson *et al.*[39] We find good agreement between the theoretical and experimental formation enthalpies with the largest discrepancy less than 1 kJ/mol. We also note that the positive formation enthalpy for the random alloy is normally an indication of (but does not guarantee) a phase-separating tendency in this sys-

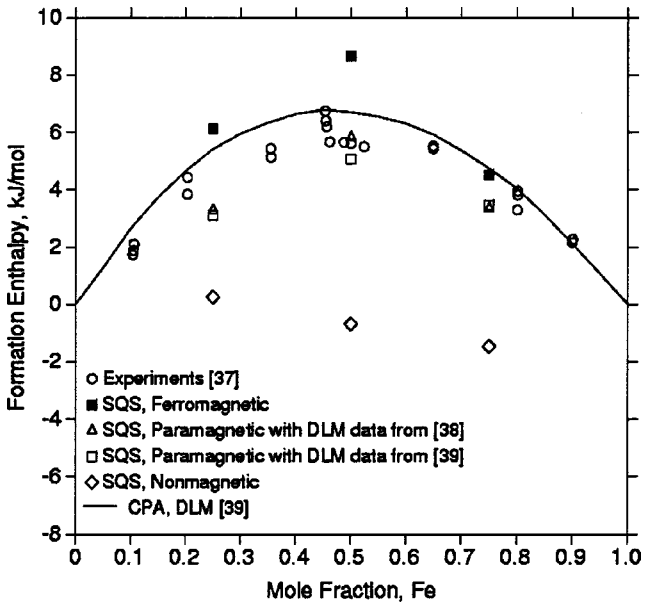

FIG. 9. Theoretical and experimental formation enthalpies of Cr–Fe bcc alloys as a function of composition. The SQS paramagnetic results are obtained by adding $\Delta H^{\mathrm{FM}\rightarrow\mathrm{PM}}$ (from Refs. 38 and 39, respectively) to our SQS calculated formation enthalpies of ferromagnetic Cr–Fe bcc alloys.

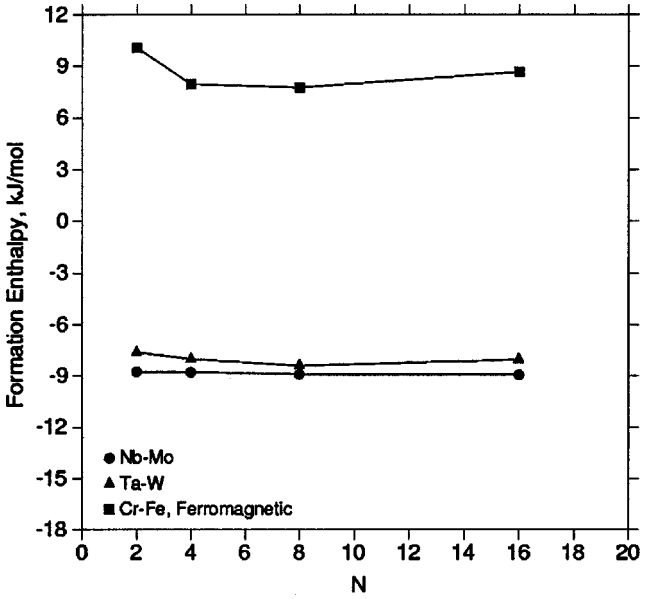

FIG. 10. SQS calculated formation enthalpies of Nb–Mo, Ta–W and Cr–Fe bcc alloys at $x=0.5$ as a function of N, the number of atoms per unit cell.

tem, consistent with the observed miscibility gap.[32]

Non-spin-polarized calculations were also performed on the present SQS's, which, however, predicted the wrong sign of the formation enthalpies, as shown in Fig. 9. Thus, we can conclude that the nonmagnetic calculations are a particularly poor representation of the paramagnetic state for these alloys.

E. Convergence tests

Figure 10 gives the formation enthalpies of various SQS-N structures for $x=0.5$ with $N=2$, 4, 8 and 16 atoms per unit cell, respectively. For all three systems considered in the present study, we observed a rapid convergence of the SQS calculated formation enthalpies with respect to N. Remarkably, in Mo–Nb and Ta–W, even calculations on SQS-2 predicted well within 1 kJ/mol the results obtained using SQS-16. From Table III, we see that even the SQS-2 has a nearest-neighbor correlation which matches that of the random alloy precisely. Thus, the rapid convergence of SQS-N with respect to N in for Mo–Nb and Ta–W could be an indication that the energetics of these alloy systems are dominated by nearest-neighbor pair interactions. In Cr–Fe, the convergence is still rapid, though somewhat less so, possibly due to the magnetic effects. Similar rapid convergence behavior of the fcc SQS's were also observed by Zunger *et al.*[3,4]

F. Bond lengths in random alloys

In Fig. 11, the average nearest neighbor A–A, A–B and B–B bond lengths in random Mo–Nb, Ta–W and Cr–Fe bcc alloys are presented. In all systems, our results clearly show three distinct nearest neighbor bond lengths R_{A-A}, R_{A-B} and R_{B-B} at all compositions, all deviating from that of the average lattice, i.e., $R=\sqrt{3}/2a, a$ being the equilibrium lattice pa-

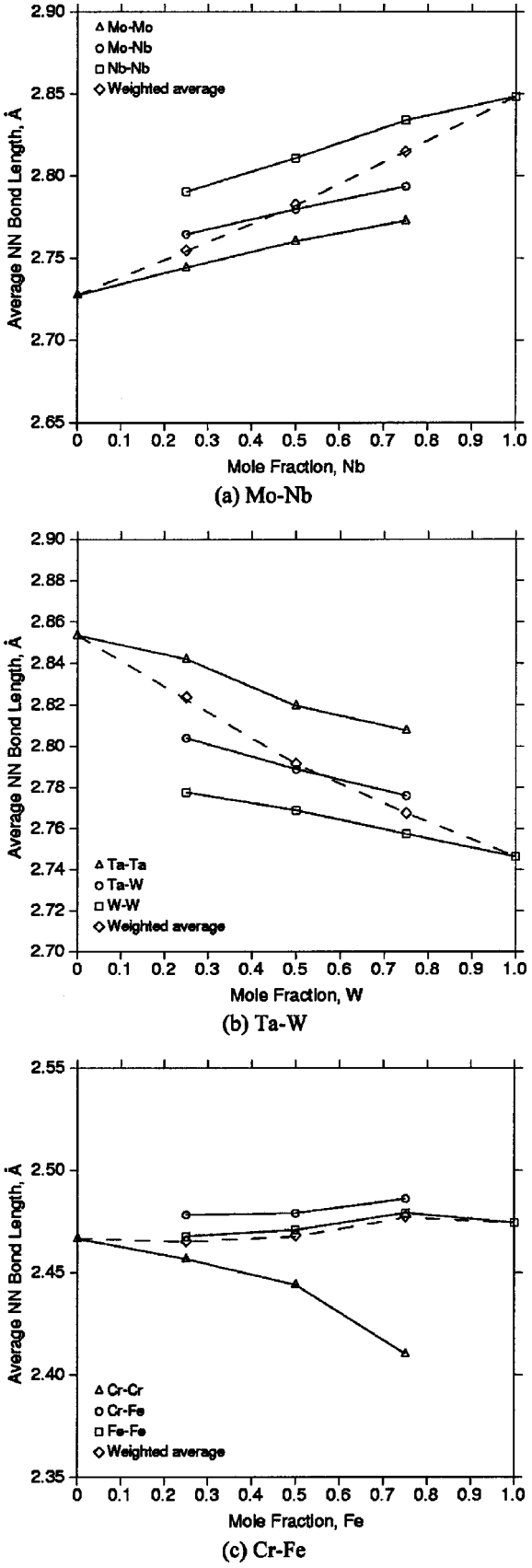

FIG. 11. SQS calculated average nearest-neighbor bond lengths as a function of composition in random bcc alloys. The dashed lines represent the average lattice.

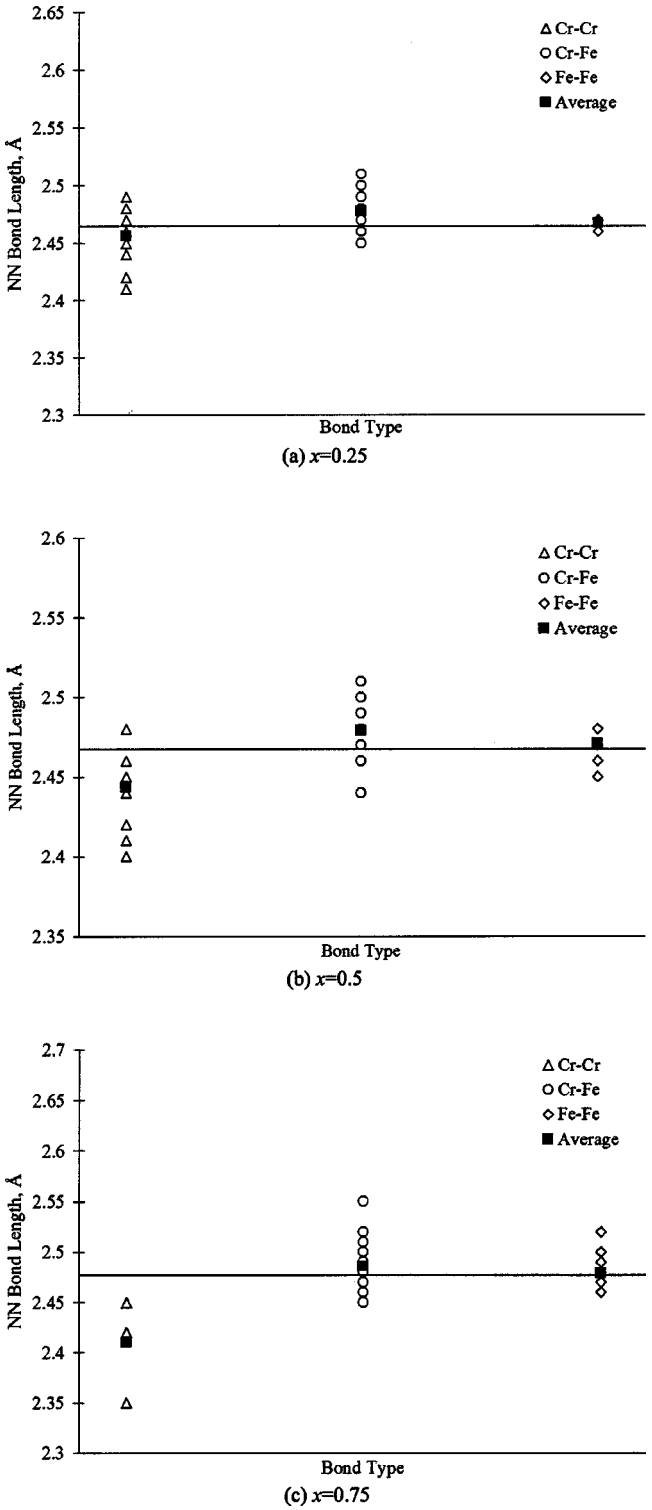

FIG. 12. SQS calculated nearest neighbor bond length distributions in random $Cr_{1-x}Fe_x$ bcc alloys at compositions (a) $x=0.25$, (b) $x=0.5$ and (c) $x=0.75$. The horizontal lines correspond to the average bcc lattice.

rameter of the alloy. Nevertheless, the weighted average of these bond lengths, i.e., $x_A^2 R_{A-A} + 2x_A x_B R_{A-B} + x_B^2 R_{B-B}$, do follow R, as shown by the dashed lines in Fig. 11. In the Mo–Nb and Ta–W systems, the bond lengths follow the "expected" behavior in that the bonds between unlike atoms are intermediate between the large–large and small–small like atom bonds.

However, the relaxation behavior of Cr–Fe is somewhat unexpected: Even though the Cr–Fe system is a perfectly lattice-matched system, the average Cr–Cr, Cr–Fe and Fe–Fe bond lengths are actually quite different. Thus, in this system, the atomic relaxation is not simply mediated by traditional atomic size mismatch considerations, but must also have a contribution due to electronic or band structure effects. We see that a small lattice-mismatch does not necessarily guarantee small atomic relaxation, as is often asserted. We find the average Cr–Fe bond length to be larger than those of both Cr–Cr and Fe–Fe bonds. To further investigate this issue, we also give in Fig. 12 the predicted nearest neighbor bond length distributions in Cr–Fe bcc alloys. The horizontal lines correspond to the average bcc lattice. As shown, there exists a dispersion of bond lengths for all three types of bonds, i.e., Cr–Cr, Cr–Fe and Fe–Fe, indicating the existence of local lattice relaxations. This unusual structural behavior of the Cr–Fe bcc alloys is interesting in light of the phase-separating tendency in this system: a miscibility gap is experimentally observed in this system at low temperatures.[32]

V. SUMMARY

We proposed three 16-atom SQS supercells to mimic the pair and multisite correlation functions of random binary bcc substitutional alloys. In each of them, a distribution of distinct local environments is created, the average of which corresponds to the random alloy. Those SQS's were then applied to predict the lattice parameters, formation enthalpies, magnetic moments and bond lengths of Mo–Nb, Ta–W and Cr–Fe bcc alloys, and the results are in good agreement with the experimental data in the literature, when available. The magnetic effects were found to be significant in Cr–Fe, and a combination of our ferromagnetic SQS calculations with previous calculations on the paramagnetic state result in formation energies that agree well with experimental measurements. The convergence tests showed that 16-atom SQS's provide good approximations of the real random solutions, and even very small 2-atom SQS's provide reasonably accurate energetics. Thus, this two-atom structure could be used as a very simple "screen" for bcc random alloy energetics. The calculated nearest neighbor bond lengths showed that, even in perfectly lattice-matched systems such as Cr–Fe, the average A–A, A–B and B–B bond lengths can be quite different. Finally, the presently proposed SQS's are general and can be applied to other binary bcc alloys.

ACKNOWLEDGMENTS

The authors wish to thank Dr. Axel van de Walle for his kind help on the use of the ATAT software package. The Materials Simulation Center (MSC) at Pennsylvania State University is also acknowledged for providing computing facilities. This work is funded by the National Science Foundation through the Information Technology Research Grant No. DMR-0205232.

[1] W. Kohn and L. Sham, Phys. Rev. **140**, 1133 (1965).
[2] B. L. Gyorffy, Phys. Rev. B **5**, 2382 (1972).
[3] A. Zunger, S. H. Wei, L. G. Ferreira, and J. E. Bernard, Phys. Rev. Lett. **65**, 353 (1990).
[4] S. H. Wei, L. G. Ferreira, J. E. Bernard, and A. Zunger, Phys. Rev. B **42**, 9622 (1990).
[5] Z. W. Lu, S. H. Wei, and A. Zunger, Phys. Rev. B **44**, 3387 (1991).
[6] Z. W. Lu, S. H. Wei, and A. Zunger, Phys. Rev. B **45**, 10 314 (1992).
[7] A. V. Ruban, S. I. Simak, S. Shallcross, and H. L. Skriver, Phys. Rev. B **67**, 214302 (2003).
[8] J. C. Mikkelsen and J. B. Boyce, Phys. Rev. Lett. **49**, 1412 (1982).
[9] K. C. Hass, L. C. Davis, and A. Zunger, Phys. Rev. B **42**, 3757 (1990).
[10] V. Ozolins, C. Wolverton, and A. Zunger, Phys. Rev. B **57**, 6427 (1998).
[11] C. Wolverton, Acta Mater. **49**, 3129 (2001).
[12] A. van de Walle, M. Asta, and G. Ceder, CALPHAD: Comput. Coupling Phase Diagrams Thermochem. **26**, 539 (2003).
[13] H. T. Stokes and D. M. Hatch, FINDSYM, www.physics.byu.edu/~stokesh/isotropy.html, 2001.
[14] D. Vanderbilt, Phys. Rev. B **41**, 7892 (1990).
[15] G. Kresse and J. Hafner, J. Phys.: Condens. Matter **6**, 8245 (1994).
[16] G. Kresse and J. Furthmuller, Phys. Rev. B **54**, 11 169 (1996).
[17] G. Kresse and J. Furthmuller, Comput. Mater. Sci. **6**, 15 (1996).
[18] J. P. Perdew, J. A. Chevary, S. H. Vosko, K. A. Jackson, M. R. Pederson, D. J. Singh, and C. Fiolhais, Phys. Rev. B **46**, 6671 (1992).
[19] C. Amador, W. R. L. Lambrecht, and B. Segall, Phys. Rev. B **46**, 1870 (1992).
[20] H. J. Monkhorst and J. D. Pack, Phys. Rev. B **13**, 5188 (1972).
[21] P. G. Evans, E. D. Isaacs, G. Aeppli, Z. Cai, and B. Lai, Science **295**, 1042 (2002).
[22] N. Kimura and Y. Kakehashi, J. Magn. Magn. Mater. **226-230**, 1019 (2001).
[23] E. Fawcett, H. L. Alberts, V. Y. Galkin, D. R. Noakes, and J. V. Yakhmi, Rev. Mod. Phys. **66**, 25 (1994).
[24] S. C. Singhal and W. L. Worrell, Metall. Trans. **4**, 1125 (1973).
[25] H. J. Goldschmidt and J. A. Brand, J. Less-Common Met. **3**, 44 (1961).
[26] J. A. Catterall and S. M. Barker, Plansee Proceedings, 1964, p. 577.
[27] C. Sigli, M. Kosugi, and J. M. Sanchez, Phys. Rev. Lett. **57**, 253 (1986).
[28] S. C. Singhal and W. L. Worrell, Metall. Trans. **4**, 895 (1973).
[29] R. Krishnan, S. P. Garg, and N. Krishnamurthy, J. Alloy Phase Diagrams **3**, 1 (1987).
[30] P. E. A. Turchi, A. Gonis, V. Drchal, and J. Kudrnovsky, Phys. Rev. B **64**, 085112 (2001).
[31] N. K. Arkhipova, S. M. Klotsman, I. P. Polikarpova, G. N. Tatarinova, A. N. Timofeev, and L. M. Veretennikov, Phys. Rev. B **30**, 1788 (1984).
[32] V. P. Itkin, in *Phase Diagrams of Binary Iron Alloys*, edited by H. Okamoto (ASM International, Materials Park, OH, 1993), p. 102.
[33] G. D. Preston, Philos. Mag. **13**, 419 (1932).
[34] A. T. Aldred, Phys. Rev. B **14**, 219 (1976).
[35] Y. A. Dorofeyev, A. Z. Menshikov, and G. A. Takzey, Phys. Met. Metallogr. **55**, 102 (1983).
[36] N. I. Kulikov and C. Demangeat, Phys. Rev. B **55**, 3533 (1997).
[37] W. A. Dench, Trans. Faraday Soc. **59**, 1279 (1962).
[38] H. Akai and P. H. Dederichs, Phys. Rev. B **47**, 8739 (1993).
[39] P. Olsson, I. A. Abrikosov, L. Vitos, and J. Wallenius, J. Nucl. Mater. **321**, 84 (2003).